Título artículo / Títol article:	45S5 bioactive glass coatings by atmospheric plasma spraying obtained from feedstocks prepared by different routes
Autores / Autors	López, Verónica ; Vicent, Mónica ; Bannier, Emilie ; Cañas Recacha, Eugeni ; Boccaccini, Aldo R. ;Cordero Arias, L. ; Sánchez Vilches, Enrique Javier
Revista:	Journal of Materials Science December 2014, Volume 49, Issue 23
Versión / Versió:	Preprint de l'autor
Cita bibliográfica / Cita bibliogràfica (ISO 690):	CALVO, Verónica López, et al. 45S5 bioactive glass coatings by atmospheric plasma spraying obtained from feedstocks prepared by different routes. Journal of Materials Science, 2014, 49.23: 7933-7942.
url Repositori UJI:	http://hdl.handle.net/10234/127366

45S5 bioactive glass coatings by atmospheric plasma spraying obtained from feedstocks prepared by different routes

Verónica López [(a)], Mónica Vicent [(a,*)], Emilie Bannier [(a)], Eugeni Cañas [(a)], Aldo R. Boccaccini [(b)], Luis Cordero [(b)], Enrique Sánchez [(a)]

[(a)] Instituto de Tecnología Cerámica (ITC), Asociación de Investigación de las Industrias Cerámicas (AICE), Universitat Jaume I (UJI), Castellón, Spain

[(b)] Institute of Biomaterials, Department of Materials Science and Engineering, University of Erlangen-Nuremberg (FAU), Erlangen, Germany

Mónica Vicent Cabedo
Email: monica.vicent@itc.uji.es Telephone number: (+34) 964342424
Fax number: (+34) 964342425

Verónica López Calvo
Email: velocal22@gmail.com

Emilie Bannier
Email: emilie.bannier@itc.uji.es

Eugeni Cañas Recacha
Email: ecanas@uji.es

Aldo R. Boccaccini
Email: aldo.boccaccini@ww.uni-erlangen.de

Luis Cordero Arias
Email: luis.cordero@studium.uni-erlangen.de

Enrique Sánchez Vilches
Email: enrique.sanchez@itc.uji.es

Abstract

45S5 bioactive glass powders with the following composition: 45 wt% SiO_2, 6 wt% P_2O_5, 24.5 wt% CaO and 24.5 wt% Na_2O were melted and quenched in water to obtain a frit. The frit was milled using two different routes: dry milling followed by sieving to obtain glass particles, and wet milling followed by spray drying to obtain a powder comprising porous agglomerates. All feedstocks showed adequate characteristics that make them suitable to be deposited by atmospheric plasma spraying. The powders and coatings were characterised by field-emission gun environmental scanning electron microscope and X-ray diffraction. The roughness and the contact angle of the coatings were also determined. The bioactivity of the powders and coatings was assessed by immersion in Simulated Body Fluid. It was found that bioactive glass prepared from bioglass frit by dry milling exhibited similar bioactivity as that of a commercial bioactive glass. All coatings produced showed good adhesion to the substrate as well as suitable surface properties to ensure efficient contact with body fluid. Regardless the characteristics of the feedstocks or plasma spray conditions used, all coatings were exclusively made up of an amorphous phase. On the other hand micrographs revealed that the characteristics of the feedstock strongly impact on the final coating microstructure. The most homogeneous microstructure was obtained when the feedstock was prepared by fine dry grinding of the frit. For this coating the formation of a bioactive layer was also proved by Fourier transform infrared spectroscopy and X-ray diffraction.

Keywords: Atmospheric plasma spraying; Feedstock preparation; Biomedical coatings; 45S5 Bioactive glass

1. Introduction

Bioactive glasses (BGs) can be used in biomedical applications as coatings for prosthetic metallic implants because of their high bioactivity and osteoconductivity [1]. The first bioactive glass, developed by Hench et al was 45S5 Bioglass® [2], which has the following composition: 45 wt% SiO_2, 6 wt% P_2O_5, 24.5 wt% CaO and 24.5 wt% Na_2O. This material is biocompatible and exhibits a strong interfacial bonding with bone. It is now well-established that when BGs are placed in contact with physiological fluids a hydroxycarbonated apatite (HCA) layer that is very similar to mineral bone composition, grows on their surface [3]. This growth is attributed to BG bioactivity [4].

The bioactivity is in turn related to a complexation-exchange mechanism on the surface of BGs in direct contact with the surrounded fluids. The bioactivity is influenced by the composition and synthesis route of BG powder [5, 6].

To obtain bioactive glass powders there are two well extended techniques: melting and subsequent crushing of a (usually) crystalline powder mixture and the sol-gel technique [6, 7]. When the sol-gel method is used, the starting materials are processed at lower temperature giving rise to bioactive glasses that exhibit higher bioactivity and biodegradability in comparison with glasses obtained by the melting procedure [8, 9]. To show bioactivity, the limit SiO_2 content for bioactive glasses is circa 90 mol% for sol-gel derived glasses and about 60 mol% for melt-derived method [10, 11]. However the melting method shows significant advantages, namely: lower cost and environmental impact, simpler scale-up and better mechanical properties of the final coating [5, 6].

On the other hand bioactive glass powders must be deposited on the substrate, usually metallic alloys, in order to obtain bioactive glass coatings as required by the final implant application. Although there are many potential coating techniques to obtain BG coatings, Atmospheric Plasma Spraying (APS) is perhaps the most popular technique due to the good mechanical performance (bond strength and mechanical properties) together with an excellent preservation of the amorphous structure of the glass powder feedstock [12, 13].

This study focuses on the preparation and optimisation of BG powders for APS feedstocks using two different preparation routes by the melting procedure: (1) dry milling followed by sieving to obtain solid pellets (“Dry Route”, referred as DR) and (2) wet milling followed by spray drying to obtain a powder comprising porous agglomerates (“Wet Route”, referred as WR). Thus the study addresses the comparison between coatings obtained from both different routes. All feedstocks were characterised in terms of microstructure and flowability as well as by immersion tests in Simulated Body Fluid (SBF) to detect bioactivity. Next coatings were obtained from these feedstocks at different plasma spraying conditions. The coatings were also microstructurally characterised to compare the impact of the feedstock characteristics. Finally some coatings were also characterised by inmersion in SBF.

In all cases (feedstocks or coating samples) the results of SBF method were monitored by Fourier Transform Infrared Spectroscopy (FTIR) and X-ray diffraction (XRD) techniques.

2. Experimental

2.1. Feedstock preparation

Feedstocks of 45S5 Bioglass® referred as BG were prepared by melting a mixture of analytical grade SiO_2, Ca_3PO_4, $NaCO_3$ and $CaCO_3$ in a furnace (SPL 4028, Carbolite Ltd, UK). The applied thermal cycle was: from room temperature to 1100 ºC at 10 ºC min^{-1}; 1 h at 1100 ºC; from 1100 ºC to 1450 ºC at 10 ºC min^{-1}; and finally 30 min at 1450 ºC. The melt was then quenched in water obtaining the frit. The chemical composition of the frit was determined by wave length dispersion X-ray fluorescence spectrometry (AXIOS, PANalytical, Netherlands). The frit was subsequently milled following two different routes: dry and wet method. In the DR method the frit was ground in a hammer mill and the resulting powder was sieved to obtain two powder fractions which were then used as APS feedstocks: 125-63 μm (referred as **DR 125-63**) and the 63 μm undersize (referred as **DR 63**).

A different procedure was used to obtain the feedstock in the WR. In this case a BG suspension was prepared in distilled water by milling the water-frit mixture in a planetary ball milling containing spherical grinding media of stabilised zirconia. The particle size distribution of this ground frit was: 100 wt% of 63 μm undersize and D_{50} = 2.2 μm. A commercial polyacrylic acid-based polyelectrolyte (DURAMAX™ D-3005, Rohm & Haas, USA) was used as dispersant [14]. A stable, 40 wt% solid content suspension of wet milled BG particles was then prepared. This suspension was characterised and the results of viscosity, density and pH were: ≤ 1000 mPa·s, 1.3 g cm^{-3} and 12.7, respectively.

This suspension was granulated in a spray dryer (Mobile Minor, Gea Niro, Denmark) to obtain a powder comprising porous agglomerates (hereafter referred as **WR** sample) [14, 15]. This was the third APS feedstock investigated in this study.

2.2. Feedstock characterisation techniques

A Field-Emission Gun Environmental Scanning Electron Microscope (FEG-ESEM) was used to analyse the feedstock microstructure (QUANTA 200FEG, FEI Company, USA). Granule size distribution was measured by dry sieving. The powder flowability was assessed by determining the Hausner ratio in a glass container. This ratio was defined as the quotient between tapped and apparent density of the powder as set out elsewhere [15, 16]. For the spray-dry powder the granule density was estimated from tapped powder density by assuming a theoretical packing factor of 0.6, which is characteristic of monosized, spherical particles [15].

Finally, the powders were immersed in SBF to investigate their bioactive character according to the procedure by Kobuko [17]. Soaking times were 1, 2, 3, 5 and 7 days. During immersion, samples were placed in an orbital shaker (KS 4000i control, IKA, Germany) at 37 ºC. After SBF soaking, the glass powder was filtered, gently rinsed with distilled water and dehydrated with acetone. The samples were dried at 60 ºC for 24 h before characterisation. A commercial, Bioglass® powder (referred as **BG STD** powder) with a mean particle size of D_{50} = 4.4 μm was also tested for comparison purposes. All the tested samples were examined by FTIR (Nicolet 6700, Bruker Instruments, Germany) to investigate the possible formation of hydroxyapatite (HA) layer. The amorphous/crystalline character of the feedstocks was identified by XRD analysis using a diffractometer (Advance diffractometer, Bruker Theta-Theta, Germany) with Cu Kα radiation (λ = 1.54183 Å). The generator settings were 40 kV and 45 mA. XRD data were collected in a 2θ range of 20-90° with a step width of 0.015° and a coating time of 2 s $step^{-1}$. This technique was also used to identify crystalline compounds after the feedstocks were immersed in SBF.

2.3. Coating deposition

BG coatings were deposited by APS using the three prepared feedstocks: DR 63, DR 125-63 and WR powders. The metallic substrates (AISI 304) were grit blasted with corundum and then cleaned with ethanol before projection. The plasma spray equipment consisted of a gun (F4-MB, Sulzer Metco, Germany) operated by a robot (IRB 1400, ABB, Switzerland). Deposition was performed using argon as primary and hydrogen as secondary plasma gases. Two different set of project conditions were used: the first one was more energetic (higher plasma enthalpy) and was applied to DR 125-63 and WR

powders, the second one, less energetic (lower plasma enthalpy), was applied to all the powders. The details of all these sets of plasma spray conditions are listed in table 1.

2.4. Coating characterisation

The crystalline phases of the coatings were characterised by XRD analysis. The roughness measurements were performed by laser scanning microscope (UBM Messtechnik GmbH, microfocus compact, Germany) and the contact angles were measured with a instrument determining the wettability of the coatings (DSA30, Kruess Gmbh, Germany). The microstructure of coating surfaces and cross-sections was examined by FEG-ESEM.

Finally, the coating obtained from DR 63 powder under the low energetic spray conditions (L-DR 63 sample) was selected for immersion in SBF test at 3, 7 and 21 soaking days. SBF was prepared as set out above and the possible formation of HA was followed via FTIR and XRD.

3. Results and discussion

3.1. Feedstock characterisation

Chemical composition of the BG frit prepared in this work is detailed in table 2. As observed in this table, sodium content is slightly lower than that of the nominal 45S5 composition as a consequence of volatilisation during melting operation.

Figure 1 shows the FEG-ESEM micrographs of the DR 63, DR 125-63 and WR powders. The first two samples (corresponding micrographs a to d) exhibit the angular, typical shape of ground frit particles, while the last powder (micrographs e and f) shows the characteristic spherical morphology of spray dried agglomerates [15]. As it can be seen these agglomerates display high porosity. The presence of the inner hole in some typical doughnut-shaped agglomerates is also observed. Particle size distribution measured by sieving, Hausner ratio and particle apparent density for the three feedstocks are given in table 3. As expected, the particle size distribution of WR powder is wider and the average particle size is coarser than those of the DR powders due to the granulated nature of WR sample. For this reason the flowability of WR powder as represented by the Hausner ratio is much higher (lower Hausner ratio) due to its coarser particle size and round morphology of its agglomerates. An approximate flowability

threshold for free-flowing powders in terms of Hausner ratio is about 1.25 [16]. Thus the flowability of the finer DR powder (DR 63) is limited. In addition, the agglomerate density of WR powder is much lower than that of the bioactive glass powder, which is around 2.71-2.82 g cm^{-3} due to the high porosity of the spray dry granules as seen above (the estimated agglomerate porosity is about 55%) [19]. Although porous agglomerates are to be expected after a spray-drying operation, in this particular case, the spray-dried granules obtained were highly porous as a consequence of poor packing of the particle size distribution of the ground frit particles. In any case, for the three feedstocks the particle/agglomerate density overcomes the requirements established by the plasma process in relation to the incorporation of the feedstock particles into the plasma torch (density > 1000 kg m^{-3}) [20].

FTIR results from BG STD, DR 63 and WR powders before and after soaking into SBF are presented in figure 2. For the three samples without any treatment in SBF, the FTIR spectra exhibited Si-O-Si stretching bands. The band around ~1070 cm^{-1} corresponds to the vibration mode of the asymmetric stretch of Si-O-Si while the band at ~930 cm^{-1} is assigned to the stretching of Si-O (non-bonding oxygen) groups [21]. The broad peak observed at around 1450 cm^{-1} can be assigned to the band of the carbonates (CO_3^{2-}) adsorbed on surfaces [18]. As it can be observed, the IR spectra of the as-prepared samples (DR63 and WR) is quite similar to that of the BG STD sample as a consequence of the fact that all the samples are based on the same glass composition (45S5 type).

As it has been extensively reported in the literature the bands at ~580 cm^{-1} and ~610 cm^{-1} correspond to bending of PO_4^{3-} groups which indicate the apatite formation in SBF [18, 22]. Thus, for BG STD sample these bands are visible at 2 days, for DR 63 powder at 3 days and finally for WR sample at 5 days. Additionally, there is a peak at ~1090 cm^{-1} that is attributed to the stretching of PO_4^{3-} groups. For BG STD sample this peak is more attenuated than those of the other two powders. On the other hand peaks at ~880 cm^{-1} and ~970 cm^{-1} indicate the presence of HPO_4^{2-} [23]. These findings show that bioactive glass feedstocks developed in this work exhibit bioactivity similar to that observed in a commercial bioactive glass. The formation of HA film occurs at different soaking times though. Thus despite the fact that DR and WR feedstocks were prepared from the same BG frit the feedstock processed by the wet route (WR) displayed a

delayed response in comparison with the sample processed by dry grinding. The interaction between BG frit particles surface and water which always occurs during wet milling seems to affect the following reaction between the glass powder and the SBF mixture. Hence FTIR data demonstrates that the powder preparation route can impact on the bioactivity response of the resulting feedstock.

XRD patterns of BG STD, DR 63 and WR powders after being soaked in SBF for 7 days are shown in figure 3. For the sake of comparison, the spectrum of the as-prepared BG frit is also included in this figure. This last spectrum can be considered as the reference for the three feedstocks since all of them share the same chemical composition (45S5 type). As it can be seen, hydroxyapatite formation is confirmed in the three feedstocks. However clear differences are again observed between the two feedstocks prepared in this work. The diffractogram of the DR 63 looks much like that of the BG STD in which the evolution of crystalline HA layer is evident. However the HA peaks in the WR sample is much more incipient confirming the delayed response of this sample when is immersed in SBF as set out above. Therefore a good correlation between XRD and FTIR analysis has been observed.

3.2. Coating characterisation

Figure 4 shows one of the results of XRD analysis of a bioglass coating (L-DR 63). The other coatings showed similar diffractograms. Thus in the bioglass coatings obtained in this research the amorphous structure of the feedstocks is preserved regardless the plasma spraying conditions used. As reported elsewhere high cooling rates are necessary to prevent recrystallisation and to obtain amorphous phase provided that the plasma torch temperature overcomes the recrystallisation point of the bioactive glass (650-700 ºC) [22]. As the diffractograms reveal, these conditions were achieved by the plasma deposition in all the experiments. As extensively set out in the literature the preservation of this amorphous structure seems to be a key issue in order to enhance bioactivity response [24].

The FEG-ESEM micrographs of the microstructure of all coatings obtained are presented in figure 5. Pictures show typical microstructure of plasma sprayed coating comprising a splat-based matrix which includes cracks, pores and unmelted feedstock particles [25]. As it can be seen, for a given feedstock the influence of the plasma

enthalpy on the final coating microstructure is not very appreciable. However the characteristics of the feedstocks strongly affect the coating microstructure. The micrographs obtained from the spray-dried powder (samples L-WR and H-WR) reveal a quite heterogeneous microstructure made up of a great deal of large, round pores trapped inside the splats. In addition, some inter-splats cracks are visible throughout the matrix. This characteristic microstructure is mainly due to the high porosity of the spray-dried agglomerates of this feedstock. During the plasma torch travel the surface of the spray-dried agglomerates heats and melts, but heat hardly can reach the agglomerate core as a consequence of the high porosity of the agglomerates as well as the low conductivity of glass feedstocks [26]. When these surface-molten agglomerates impact on the substrate splats form which exhibit limited deformation capability due to the low melting degree (very high viscosity) inside the agglomerates. This poor deformation gives rise to high coating roughness as evidenced by FEG-ESEM observations, in particular in the coating obtained at high plasma energy conditions (H-WR) where the agglomerate contour is clearly visible on the coating surface.

Micrographs of coated samples obtained from the feedstocks prepared from dry ground bioglass (samples L-DR 125-63, H-DR 125-63 and L-DR 63) also reveal great differences in terms of microstructure. In the coating obtained from the coarser feedstock at lower plasma enthalpy (L-DR 125-63) the microstructure is basically formed by a matrix of large, relatively undeformed splats which are mostly associated with feedstock particles. Again the effect of the low glass feedstock thermal conductivity, in particular when coarse particles are used, is playing a key role in splat formation. Large round pores are also predominant in this microstructure. More importantly most of the coarse splats are surrounded by peripherical, inter-splat cracks which result in poor coating cohesion [27]. Moreover these coarse splats give rise to high surface roughness. A similar microstructure is depicted by the coating obtained at high plasma energy conditions. Finally, the coating obtained from the finer dry ground bioglass feedstock (DR 63) shows a quite homogeneous microstructure comprising a well molten matrix containing round pores. Although the matrix also contains trapped pores they are smaller and less numerous than those of the other two types of coatings. But more importantly there are few cracks in the matrix. Thus the smaller splat size of the DR 63 feedstock in comparison with the DR 125-63 sample decreases the

temperature gradient during the splat cooling on the substrate resulting in less thermal stresses and consequently fewer amounts of inter-splat cracks.

The results of roughness and wettability tests are shown in table 4. Roughness (Ra) and water contact angle for the grit-blasted, bare substrate were 2.2 ± 0.1 μm and 55º respectively. Roughness values in this table confirm most of the observations given by the FEG-ESEM micrographs in figure 5. Thus WR coatings display the highest surface roughness followed by the DR 125-63 coating samples. In addition, DR 63 coating exhibits the lowest value of roughness. On the other hand, although the differences are small, coatings obtained at higher plasma energy show lower surface roughness as a consequence of an expected higher degree of splat melting. As reported in the literature, the development of a rough surface can be advantageous for bioactivity since the surface asperities promote both the adsorption of organic metabolites and the cell attachment [28]. With regard to contact angle, there is not a good correlation between roughness and contact angle data in table 4 as a consequence of the porosity of the coatings. In fact, the scatter of the contact angle is very high due to the difficulty of assessing this property on such high roughness and porous samples. In any case both parameters (roughness and contact angle) for all coatings show favourable values (hydrophilic character) so as to ensure that the SBF can suitably contact and wet the coatings [29].

FTIR results of coatings in SBF are shown in figure 6. As mentioned above, the test was carried out on the L-DR 63 coating since this sample presented the best microstructural features. As it can be seen, the band at ~1030 cm^{-1} that is attributed to the stretching of PO_4^{3-} groups, starts to be visible after 7 days exposure. At 21 days the band is fully evolved. Thus the SBF test proves that the coating is capable of developing a surface layer of HA. However the appearance of this peak takes place at longer time than that observed for the DR 63 feedstocks, as seen in figure 2. This finding agrees with recent observations reported in the literature with regard to bioglass coatings obtained by APS [29]. According to this research, which took place with different glass compositional range (without Na_2O) the overall reaction mechanism observed in SBF immersion, especially in the first days of immersion, is strongly affected by the microstructure and degree of crystallinity of the coatings. Other previous research highlighted the impact of

the coating microstructure, in particular the pore interconnectivity, on the osteointegration [22].

XRD tests were also carried out on DR 63 coating after 7 days soaking in SBF. The XRD pattern of this sample can be found in figure 4b, together with the spectrum corresponding to this same coating before exposure to SBF (Figure 4a). As it can be seen, the pattern confirms the development of the HA film on the coating. Similar XRD patterns were reported for APS coatings obtained from different bioactive glass compositions exhibiting bioactivity [30].

Finally, FEG-ESEM observation of the hydroxyapatite film developed on the DR 63 coating after 7 days SBF exposure was carried out. Figure 7 shows the corresponding micrograph obtained together with that of as-deposited DR 63 coating. The micrograph displays the HA film covering most of the coating surface (marked HA in the picture). However some darker, non-covered areas are also observed (marked SG in the picture). Energy-Dispersive X-ray Spectroscopy analysis (EDS) shown in this same figure 7, confirms that these zones are formed by silica gel which has not evolved to HA yet.

In this research, the effect of the feedstock characteristics on the final microstructure of bioactive glass coatings obtained by APS has been investigated and upon immersion in SBF the formation of the bioactive HA layer on the prepared coatings has been proved. However further research is necessary so as to relate this microstructure with the specific properties of the HA layer.

4. Conclusions

This study addressed the preparation and optimisation of bioactive glass powders for APS feedstocks using two different preparation routes by the melting procedure: dry milling followed by sieving to obtain solid pellets (dry route) and wet milling followed by spray drying to obtain a powder comprising porous agglomerates (wet route). The spray-dry powder shows an expected high flowability while the agglomerates which comprise the powder are highly porous. On the contrary, more limited flowability was found in the feedstocks obtained by dry milling, in particular with the finest dry ground powder. In all the feedstocks similar bioactivity as that exhibited by a standard bioactive glass powder was evidenced by SBF test. The research has proved the enormous impact

of the feedstocks characteristics on the bioactive glass coating microstructure. The best microstructure characterised by smaller splats and fewer pores and cracks was achieved when the fine dry ground feedstock was used. If the particle size of this feedstock is increased the amount of inter-splat cracks associated to unmelted particles strongly rises. In addition, if an agglomerated (spray-dried) feedstock is used to enhance powder flowability the agglomerates are not capable of fully melting giving rise to an impaired microstructure.

With regard to bioactivity, an exhaustive characterisation of the bioactive glass coating (DR 63) after exposure to SBF confirmed that the coating is capable of developing a surface layer of HA.

Acknowledgements

Authors wish to acknowledge KMM-VIN European Virtual Institute on Knowledge-Based Multifunctional Materials AISBL by the funding support in a mobility grant and the University Jaume I of Castellón for the support in the project P1 1B2013-69.

References

[1] Jones JR (2013) Review of bioactive glass: From Hench to hybrids, Acta Biomater 9:4457-4486.

[2] Hench LL (2006) The story of bioglass, J Mater Sci Mater Med 17:967-978.

[3] Gerhardt LC and Boccaccini AR (2010) Bioactive glass and glass-ceramic scaffolds for bone tissue engineering, Mater 3:3867-3910.

[4] Cao W and Hench LL (1996) Bioactive materials, Ceram Int 22:493-507.

[5] Lucas-Girot A, Mezahi FZ, Mami M, Oudadesse H, Harabi A and Floch ML (2011) Sol–gel synthesis of a new composition of bioactive glass in the quaternary system SiO_2-CaO-Na_2O-P_2O_5 comparison with melting method, J Non-Cryst Solids 357:3322-3327.

[6] Sepulveda P, Jones JR and Hench LL (2002) In vitro dissolution of melt-derived 45S5 and sol-gel derived 58S bioactive glasses, J Biomed Mater Res 61:301-311.

[7] Zhou Y, Li H, Lin K, Zhai W , Gu W and Chang J (2012) Effect of heat treatment on the properties of SiO_2-CaO-MgO-P_2O_5 bioactive glasses, J Mater Sci Mater Med 23:2101-2108.

[8] Saboori A, Rabiee M, Moztarzadeh F, Sheikhi M, Tahriri M and Karimi M (2009) Synthesis, characterization and in vitro bioactivity of sol-gel-derived SiO_2-CaO-P_2O_5-MgO bioglass, Mater Sci Eng C 29:335-340.

[9] Ma J, Chen CZ, Wang DG, Meng XG and Shi JZ (2010) Influence of the sintering temperature on the structural feature and bioactivity of sol-gel derived SiO_2-CaO-P_2O_5 bioglass, Ceram Int 36:1911-1916.

[10] Brink M, Turunen T, Happonen R and Yli-Urpo A (1997) Compositional dependence of bioactivity of glasses in the system Na_2O-K_2O-MgO-CaO-B_2O_3-P_2O_5-SiO_2, J Biomed Mater Res 37:114-121.

[11] Delben JRJ, Pereira K, Oliveira SL, Alencar LDS, Hernandes AC and Delben AAST (2013) Bioactive glass prepared by sol-gel emulsion, J Non-Cryst Solids 361:119-123.

[12] Ding SJ, Su YM, Ju CP and Chern Lin JH (2001) Structure and immersion behavior of plasma-sprayed apatite-matrix coatings, Biomater 22:833-845.

[13] Lee TM, Chang E, Wang BC and Yang CY (1996) Characteristics of plasma sprayed bioactive glass coatings on Ti-6Al-4V alloy: an in vitro study, Surf Coat Technol 79:170-177.

[14] Vicent M, Sánchez E, Moreno A and Moreno R (2012) Preparation of high solids content nano-titania suspensions to obtain spray-dried nanostructured powders for atmospheric plasma spraying, J Eur Ceram Soc 32:185-194.

[15] Vicent M, Sánchez E, Mallol G and Moreno R (2013) Study of colloidal behaviour and rheology of Al_2O_3-TiO_2 nanosuspensions to obtain free-flowing spray-dried granules for atmospheric plasma spraying, Ceram Int 39:8103-8111.

[16] Amorós JL, Blasco A, Enrique JE and Negre F (1987) Características de polvos cerámicos para prensado (Characteristics of ceramic powders for pressing), Bol Soc Esp Ceram Vidr 26:31-37.

[17] Kokubo T and Takadama H (2006) How useful is SBF in predicting in vivo bone bioactivity? Biomat 27:2907-2915.

[18] Mackovic M, Hoppe A, Detsch R, Mohn D, Stark WJ, Spiecker E, Boccaccini AR (2012) Bioactive glass (type 45S5) nanoparticles: in vitro reactivity on nanoscale and biocompatibility, J Nanopart Res 14:966.

[19] Sepúlveda P, Jones J and Hench LL (2001) Characterization of melt-derived 45S5 and sol-gel–derived 58S bioactive glasses, J Biomed Mater Res 58:734-740.

[20] Fauchais P, Montavon G and Bertrand G (2010) From powders to thermally sprayed coatings, J Therm Spray Technol 19:56-80.

[21] El-Kheshen AA, Khaliafa FA, Saad EA and Elwan RL (2008) Effect of Al_2O_3 addition on bioactivity, thermal and mechanical properties of some bioactive glasses, Ceram Int 34:1667-1673.

[22] Nelson GM, Nychka JA, McDonald AG (2011) Flame spray deposition of titanium alloy-bioactive glass composite coatings, J Therm Spray Technol. doi: 10.1007/s11666-011-9674-5

[23] Chen Q, Cordero-Arias L, Roether JA, Cabanas-Polo S, Virtanen S and Boccaccini AR (2013) Alginate/Bioglass® composite coatings on stainless steel deposited by direct current and alternating current electrophoretic deposition, Surf Coat Technol 233:49-56.

[24] Peitl Filho O, LaTorre GP and Hench LL (1996) Effect of crystallization on apatite-layer formation of bioactive glass 45S5, J Biomed Mater Res B 30:509-514.

[25] Pawlowski L (2008) The Science and Engineering of Thermal Spray Coatings 2nd edn. John Wiley & Sons

[26] Poirier T, Planche MP, Landemarre O and Coddet C (2008) Particles spreading phenomena in the case of glass thermal spraying, J Therm Spray Technol 17:564-573.

[27] Fauchais P, Montavon G, Lima RS and Marple BR (2011) Engineering a new class of thermal spray nano-based microstructures from agglomerated nanostructured particles, suspensions and solutions: an invited review, J Phys D Appl Phys 44:093001.

[28] Costa-Rodrigues J, Fernandes A, Lopes MA and Fernandes MH (2012) Hydroxyapatite surface roughness: Complex modulation of the osteoclastogenesis of human precursor cells, Acta Biomat 8:1137-1145.

[29] Cattini A, Latka L, Belluci D, Bolelli G, Sola A, Lusvarghi L, Pawlowski L and Canillo V (2013) Suspension plasma sprayed bioactive glass coatings: Effects of processing on microstructure, mechanical properties and in-vitro behaviour, Surf Coat Technol 220:52-59.

[30] Monsalve M, Ageorges H, López E, Vargas F and Bolívar F (2013) Bioactivity and mechanical properties of plasma-sprayed coatings of bioglass powders, Surf Coat Technol 220:60-66.

Tables

Table 1 Plasma spraying conditions for the three powder feedstocks prepared

Powder	ΔH[a] (MJ kg^{-1})	Coating reference	Ar (slpm)	H_2 (slpm)	I[b] (A)	d[c] (m)	v[d] (m s^{-1})
DR 125-63	35.3	H-DR 125-63	25	15	600	0.11	1
WR	35.3	H-WR					
DR 125-63	24.4	L-DR 125-63					
DR 63	24.4	L-DR 63	38	14	600	0.11	1
WR	24.4	L-WR					

slpm: standard litre per minute.

[a]Plasma average enthalpy.

[b]Arc intensity.

[c]Spraying distance.

[d]Spraying velocity.

Table 2 Nominal and as-melted oxide composition of the BG frit prepared in this work (wt%)

Composition (wt%)	SiO_2	P_2O_5	CaO	Na_2O
Nominal	45	6	24.5	24.5
As-melted	45.6	5.9	24.7	23.7

Table 3 Feedstocks' main characteristics

	Particle size distribution (μm)				Powder flowability	
Reference	d > 200 (wt%)	200 – 125 (wt%)	125 – 63 (wt%)	d < 63 (wt%)	Hausner ratio	ρ[e] (kg m^{-3})
DR 125-63	0	0	100	0	1.28 ± 0.04	NA
DR 63	0	0	0	100	1.48 ± 0.05	NA
WR[*]	10	20	70	0	1.22 ± 0.03	1250

[*]This is an agglomerated (spray-dried) powder.

[e]Agglomerate apparent density.

Table 4 Roughness (Ra) and water contact angle (º) values of coatings obtained

Feedstock	**DR 125-63**		**WR**		**DR 63**
Reference	H-DR 125-63	L-DR 125-63	H-WR	L-WR	L-DR 63
Ra (µm)	16 ± 4	16 ± 5	23 ± 5	25 ± 4	8 ± 2
Contact angle (º)	24 ± 5	31 ± 10	20 ± 10	20 ± 10	74 ± 6

Figure Captions

Fig. 1 FEG-ESEM micrographs of DR 125-63, DR63 and WR feedstocks at two different magnifications: a), b) DR 125-63, c), d) DR 63 and e),f) WR

Fig. 2 FTIR spectroscopy of BG STD and BG powders (DR 63 and WR) before and after soaking into SBF

Fig. 3 XRD patterns of BG STD, DR 63 and WR feedstocks after being soaked in SBF for 7 days. The spectrum of BG frit without SBF immersion is also included

Fig. 4 XRD patterns of: a) L-DR 63 coating showing the preserved, amorphous structure of the feedstock and b) this same coating after being soaked in SBF for 7 days

Fig. 5 FEG-ESEM micrographs of coatings obtained from the three feedstocks (WR, DR 125-63 and DR 63) at the two atmospheric plasma spray conditions: a) less energetic (L-samples) and b) more energetic (H-samples)

Fig. 6 FTIR spectra of L-DR 63 coatings: a) before soaking into SBF, b) after 3 days into SBF, c) after 7 days into SBF, d) after 21 days into SBF

Fig. 7 FEG-ESEM micrograph of as-deposited DR 63 coating (left) and the same coating after 7 days SBF exposure (right). EDS analysis results of some areas of the SBF immersed coating are shown

Figure 1

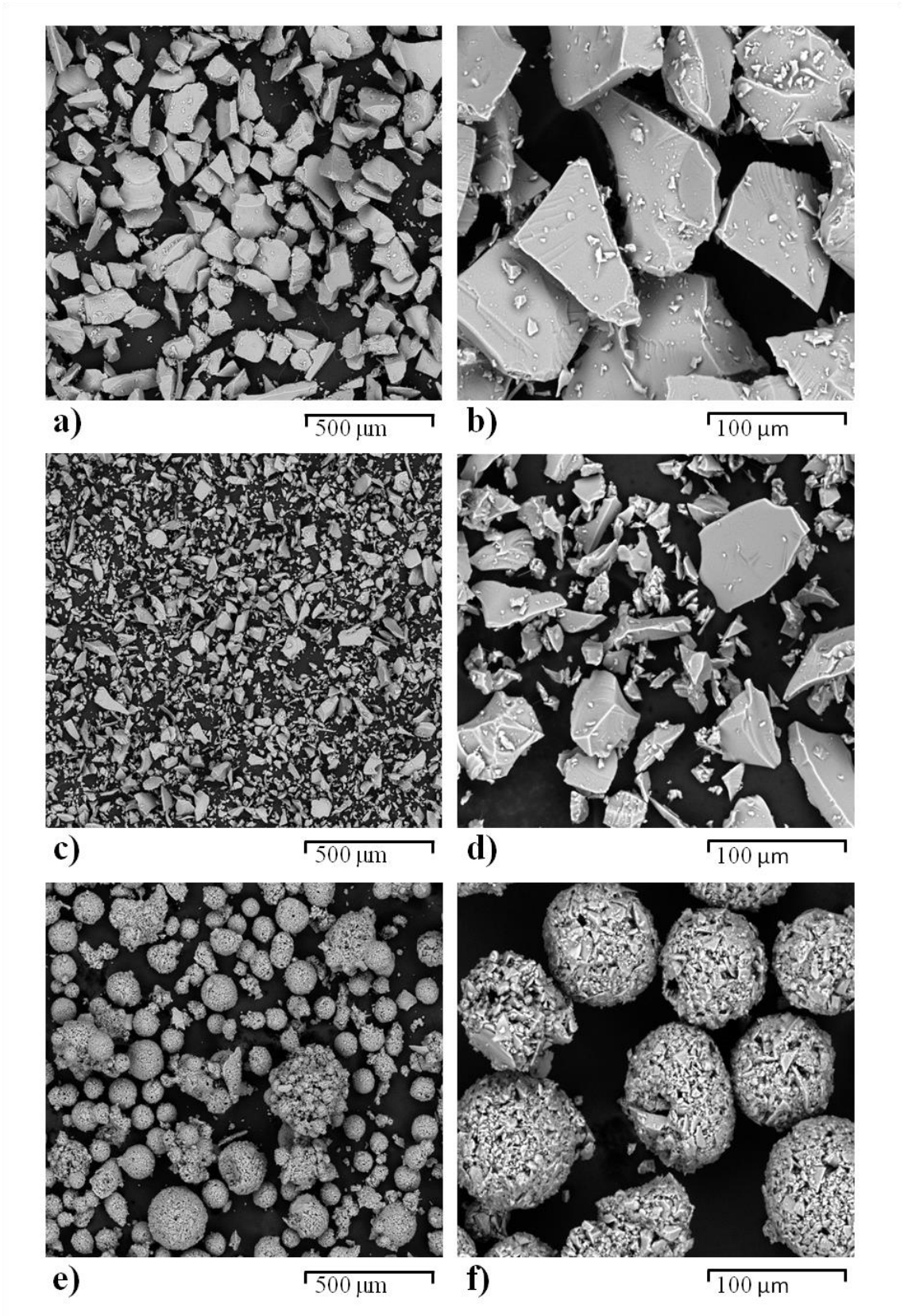

Figure 2

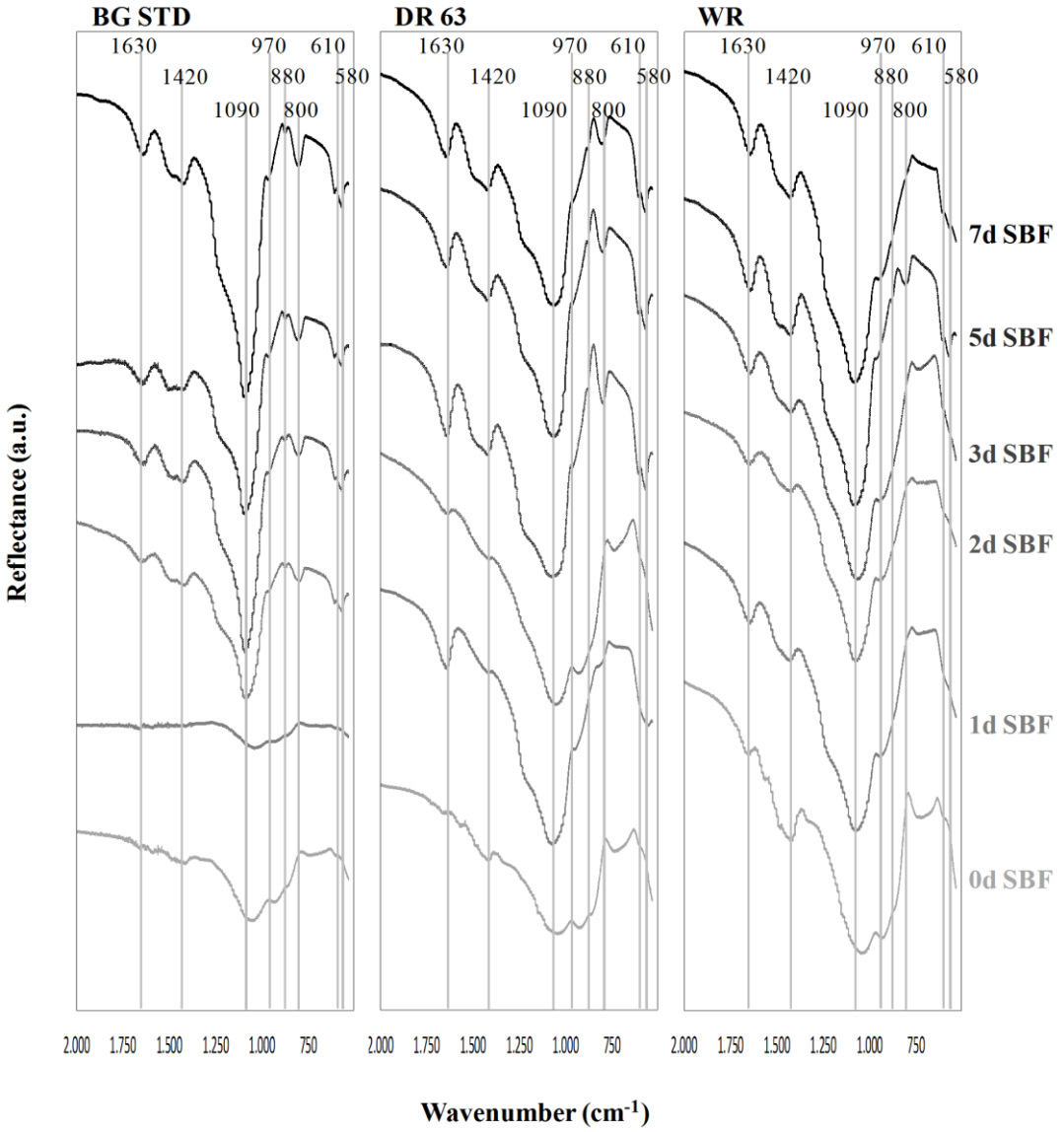
BG STD
DR 63
WR
1630
1420
1090
970
880
800
610
580
7d SBF
5d SBF
3d SBF
2d SBF
1d SBF
0d SBF
Reflectance (a.u.)
2.000
1.750
1.500
1.250
1.000
750
Wavenumber (cm-1)

Figure 3

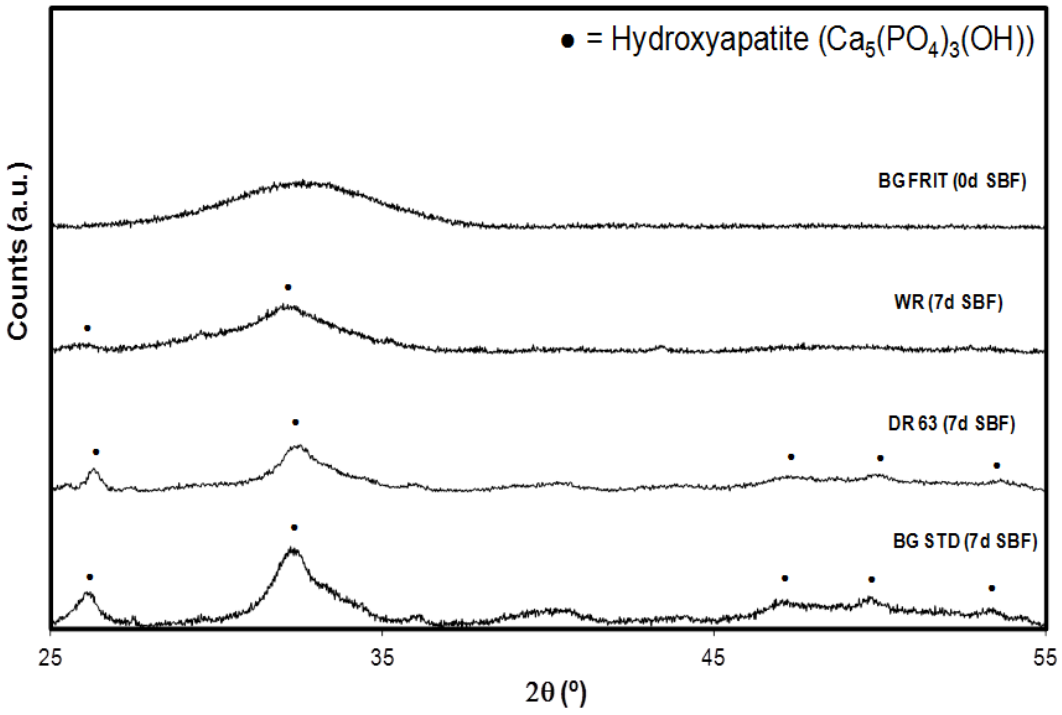
● = Hydroxyapatite ($Ca_5(PO_4)_3(OH)$)
BG FRIT (0d SBF)
WR (7d SBF)
DR 63 (7d SBF)
BG STD (7d SBF)
Counts (a.u.)
25
35
45
55
2θ (°)

Figure 4

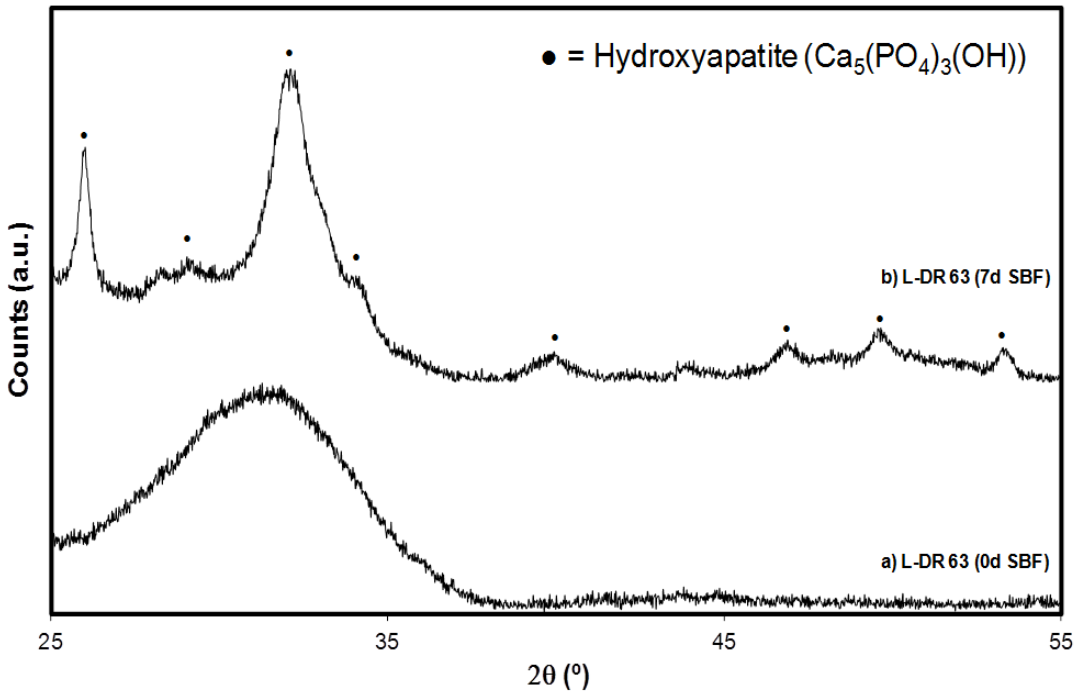
● = Hydroxyapatite ($Ca_5(PO_4)_3(OH)$)
b) L-DR 63 (7d SBF)
a) L-DR 63 (0d SBF)
Counts (a.u.)
25
35
45
55
2θ (º)

Figure 5

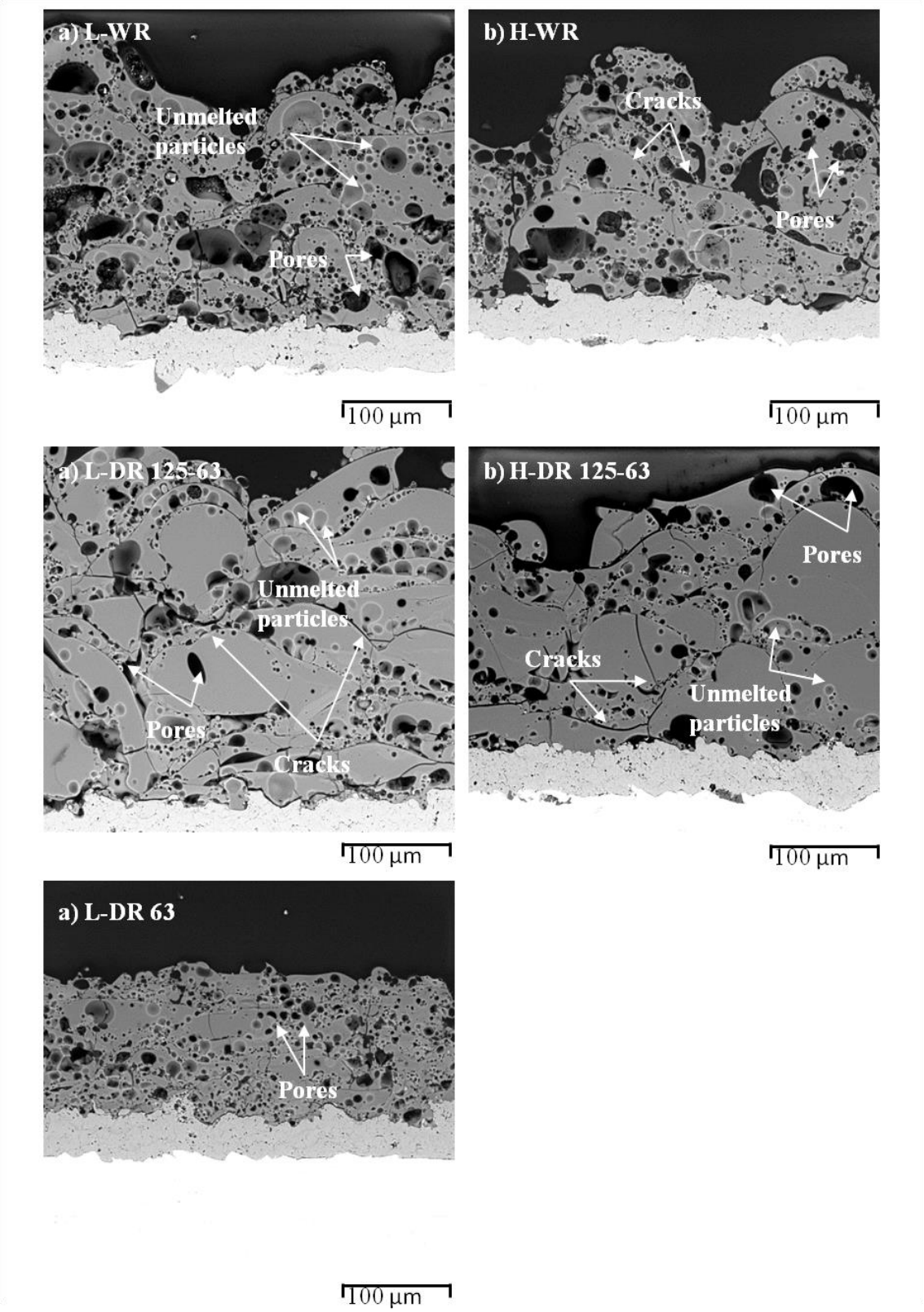
a) L-WR
Unmelted particles
Pores
100 µm
b) H-WR
Cracks
Pores
100 µm
a) L-DR 125-63
Unmelted particles
Pores
Cracks
100 µm
b) H-DR 125-63
Pores
Cracks
Unmelted particles
100 µm
a) L-DR 63
Pores
100 µm

Figure 6

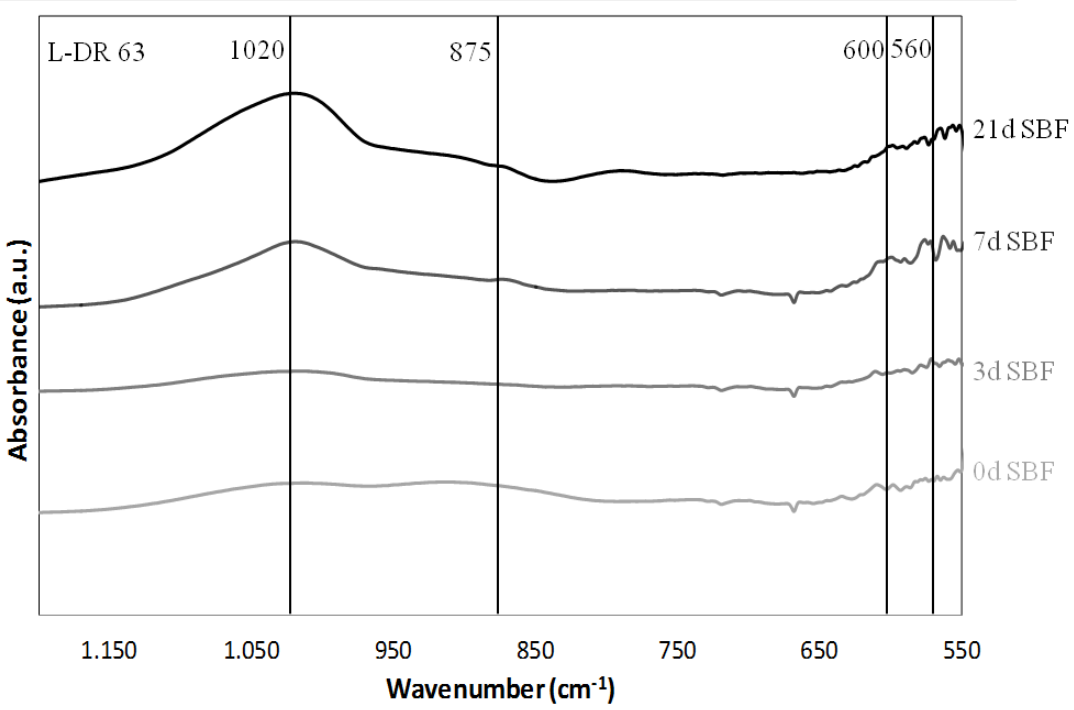
L-DR 63
1020
875
600
560
21d SBF
7d SBF
3d SBF
0d SBF
Absorbance (a.u.)
1.150
1.050
950
850
750
650
550
Wavenumber (cm-1)

Figure 7